PHYSICAL REVIEW B **75**, 220407(R) (2007)

Induced anisotropies in exchange-coupled systems on rippled substrates

M. O. Liedke,[1,2] B. Liedke,[1] A. Keller,[1] B. Hillebrands,[2] A. Mücklich,[1] S. Facsko,[1] and J. Fassbender[1,*]
[1]*Institute of Ion Beam Physics and Materials Research, Forschungszentrum Dresden-Rossendorf, P.O. Box 51 01 19, D-01314 Dresden, Germany*
[2]*Fachbereich Physik, TU Kaiserslautern, Erwin-Schroedinger-Strasse 56, D-67663 Kaiserslautern, Germany*
(Received 1 June 2007; published 25 June 2007)

The role of monoatomic steps at the mutual interface between a ferromagnetic and an antiferromagnetic layer in a $Ni_{81}Fe_{19}/Fe_{50}Mn_{50}$ exchange bias system is enlightened. For this purpose a special ripple substrate with a well defined morphology is used. Due to the film morphology a strong uniaxial anisotropy is induced in the polycrystalline $Ni_{81}Fe_{19}$ layer, which is fixed in its orientation. By means of different field annealing cycles the direction of the induced unidirectional anisotropy can be chosen. For all mutual orientations both anisotropy contributions are superimposed independently and the angular dependence of the magnetization reversal behavior can be described perfectly by a coherent rotation model with one parameter set. In addition it is demonstrated that the magnitude of the unidirectional anisotropy contribution scales with the step density of the substrate, which is in full agreement with theoretical predictions.

DOI: 10.1103/PhysRevB.75.220407 PACS number(s): 75.30.Gw, 68.35.Ct, 75.70.Cn, 75.75.+a

A thin ferromagnetic layer experiences a unidirectional anisotropy when an internal magnetic field is created due to the exchange coupling to an antiferromagnetic layer of sufficient thickness.[1,2] A shift of the hysteresis loop, the so-called exchange bias field H_{eb}, is observed if the induced internal field exhibits a well defined direction. This is conventionally achieved by a field annealing cycle, i.e., the magnetization of the ferromagnetic layer is aligned along any desired direction, when the antiferromagnetic layer is cooled down below the blocking temperature. By doing so the spin configuration of the antiferromagnetic layer is frozen and generates an internal magnetic field which acts on the ferromagnetic layer. Since in a polycrystalline film the grains are usually randomly oriented in the film plane, no higher-order anisotropies are present and the angular dependence of H_{eb} follows a simple cosine behavior, $H_{eb}(\alpha_M)=H_{eb}\times\cos(\alpha_M-\alpha_{K_1})$, as expected from a coherent rotation model. α_M (α_{K_1}) is the angle between the magnetization direction (field-cooling direction) and a reference direction. However, if higher-order anisotropy contributions are present, as, for example, magnetocrystalline contributions in epitaxial systems,[3–6] buffer induced anisotropy contributions,[7,8] or shape anisotropy contributions in patterned films,[9,10] a complicated angular dependence of the magnetization reversal behavior is observed. If in addition interfacial roughness comes into play, even more parameters enter the magnetization reversal process,[11–13] which further complicate the interpretation. In general, in experimental papers addressing the effect of interfacial roughness published so far, the amount of roughness could neither be varied easily nor quantified absolutely. Thus no consensus about the effect of interfacial roughness on the unidirectional anisotropy could be achieved.

In this Rapid Communication a special template system is used which allows us (i) to easily determine the step density and thus the interfacial roughness, and (ii) to induce a strong uniaxial anisotropy which is directly related to the highly anisotropic step distribution. Thereby we can (i) unambiguously determine the roughness induced increase in unidirectional anisotropy, and (ii) since by means of different magnetic-field annealing cycles the mutual angle between uniaxial and unidirectional anisotropy can be chosen independently, we can study their potential intercorrelation.

In order to create such a template system, self-organized ripple formation during low-energy ion erosion is employed. This process is well known for semiconductor surfaces,[14,15] where rather high topographic modulations (typically 2–20 nm) can be achieved. However, due to the ion erosion process the sample surface is amorphized. Ripple formation has also been studied for metallic surfaces and magnetic thin films.[16–18] In these cases the topographic modulations are much smaller ($\leqslant$0.2 nm) and so far these investigations are restricted to single crystalline surfaces. Therefore step-or morphology-induced anisotropy contributions are always superimposed by magnetocrystalline contributions. In order to simplify the interpretation of our results, magnetocrystalline anisotropy contributions have to be circumvented. This has been achieved by the deposition of initially low anisotropic polycrystalline $Ni_{81}Fe_{19}$ films on top of rippled Si surfaces.

The Si templates are created by 500-eV Ar^+ sputtering of a Si(001) wafer with an incident angle of 67° with respect to the surface normal in high vacuum. A sputter fluence of 1×10^{18} ions/cm^2 leads to a modulated Si surface which after deposition of a metallic buffer produces subsequently a high anisotropic step density (see Fig. 1). After ion erosion the templates have been removed from the vacuum chamber which leads to a natural oxide of 2–4 nm on the surface. Subsequent to initial atomic force microscopy (AFM) characterization the template was inserted into a molecular-beam epitaxy system. Prior to film deposition the sample was heated to 250 °C in order to clean the sample surface. Subsequently the whole layer stack, 2-nm Mn/9-nm $Ni_{81}Fe_{19}$/10-nm $Fe_{50}Mn_{50}$/2-nm Cr, was deposited at room temperature by *e*-beam evaporation (Cr, $Ni_{81}Fe_{19}$, Fe) and from a Knudsen cell (Mn), respectively. In order to compare the exchange bias system with the single ferromagnetic layer, the antiferromagnetic FeMn layer was deposited on half of the sample only. Subsequently the surface topography was reinvestigated by means of *ex situ* AFM. In order to further clarify the film morphology, cross-sectional transmission

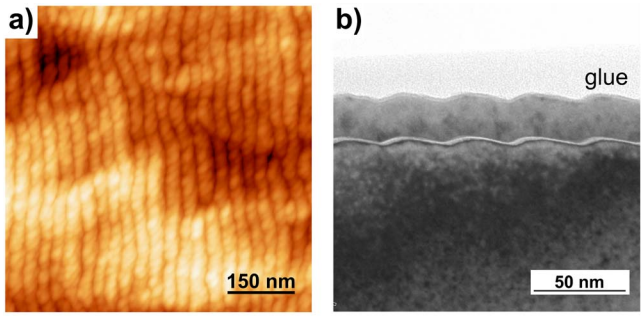

FIG. 1. (Color online) (a) AFM image of the surface topography of the exchange bias layer stack. (b) Cross-sectional TEM image of the Si ripple and metallic layer structure. The film morphology perfectly reproduces the ripple substrate.

electron microscopy (TEM) was performed for a different sample fabricated using the same recipe.

In Fig. 1(a) an AFM micrograph of the layer stack surface is shown. The ripple periodicity can be determined to $\lambda = 32$ nm from the satellite peaks observed in the two-dimensional (2D)-Fourier transform of the AFM image. A peak-to-valley height of ≈ 2 nm is observed. This corresponds to a mean local inclination of the fiber-textured (111) surface of 7°, i.e., one monoatomic step per seven atoms. The rms roughness of the ripple structure is determined to $w = 0.74$ nm. Although the metallic layer thickness is much larger than the surface corrugation of the initial template system, the ripple structure is reproduced completely with respect to periodicity and modulation amplitude. This can be observed nicely by inspection of the cross-sectional TEM image shown in Fig. 1(b).

For the interpretation of the magnetic measurements one of the crucial issues is to determine the different anisotropy contributions with the highest achievable accuracy. Therefore the whole angular dependence (360°) of the magnetization reversal behavior was measured (1° step size) and compared to numerical simulations based on a coherent rotation model which allows for the calculation of the hysteresis curves and subsequently of the angular dependence of H_{eb}. In this extended Stoner-Wohlfarth model[19,20] the free-energy density can be written as

$$f(\alpha_M) = -|\vec{M}||\vec{H}|\cos(\alpha_M - \alpha_H) - K_1 \cos(\alpha_M - \alpha_{K_1}) - K_2 \cos^2(\alpha_M - \alpha_{K_2}).$$

K_1 and K_2 are the unidirectional and uniaxial anisotropy constants, respectively, $\vec{H}$ is the applied field, and $\vec{M}$ is the magnetization. All angles α_i, corresponding to K_1, K_2, $\vec{H}$, and $\vec{M}$, are defined with respect to the ripple direction. Since this direction corresponds to the easy axis of the uniaxial anisotropy (see below), $\alpha_{K_2} = 0$. The mutual angle $\angle(K_1, K_2)$ is then only given by α_{K_1}. For the calculation of the magnetization reversal curves the perfect-delay convention is used, i.e., the magnetization remains in a local-energy minimum until the energy barrier between local and global energy minimum vanishes.

Experimentally α_{K_1} is set by applying a magnetic field of 2 kOe along different directions during a field annealing cycle. Three different configurations are discussed in the present Rapid Communication. In order to achieve a complete comparison between experimental and theoretical magnetization reversal curves a special graphical data representation is chosen. The longitudinal magnetization component is displayed color coded ($-M$: black; $+M$: white). A single hysteresis curve is displayed as a vertical line from $-H \rightarrow +H \rightarrow -H$ as indicated in Fig. 2. The experimental data are

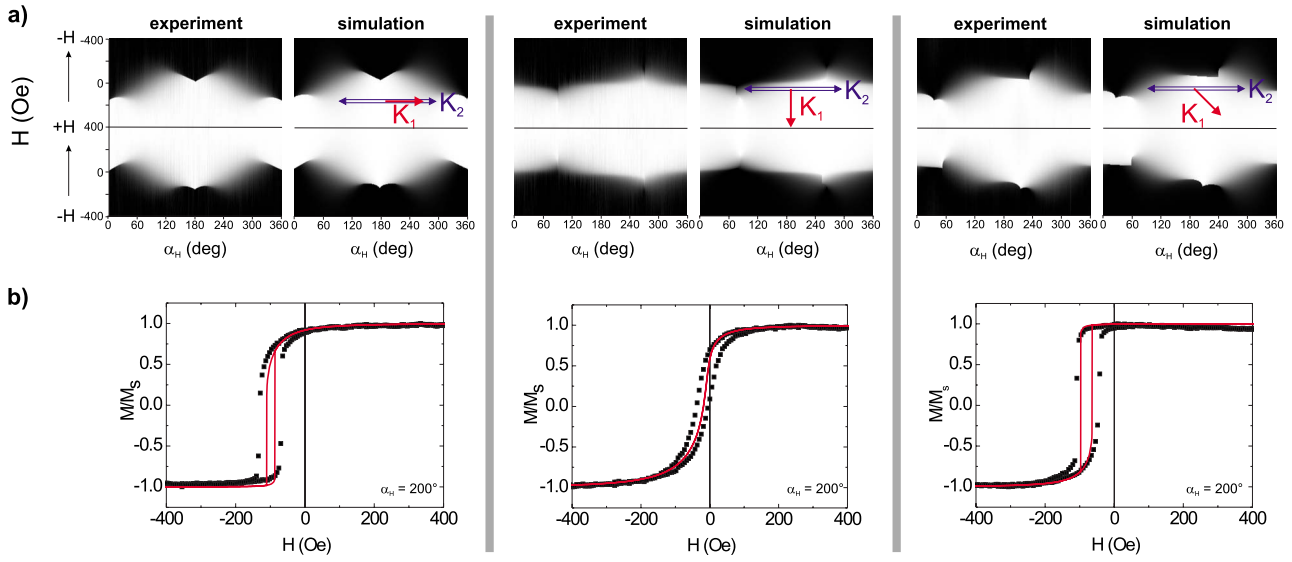

FIG. 2. (Color online) (a) Angular dependence of the magnetization reversal behavior for three different configurations (left: $\alpha_{K_1} = 1°$; middle: $\alpha_{K_1} = 86°$; right: $\alpha_{K_1} = 41°$) as sketched. In each case the left (right) image corresponds to the experimental data (simulation). The longitudinal magnetization component is displayed color coded ($-M$: black; $+M$: white). One image contains 360 hysteresis curves. (b) Conventional plots of the measured (full symbols) and simulated (line) magnetization reversal curves for $\alpha_H = 200°$ for the different configurations shown above.

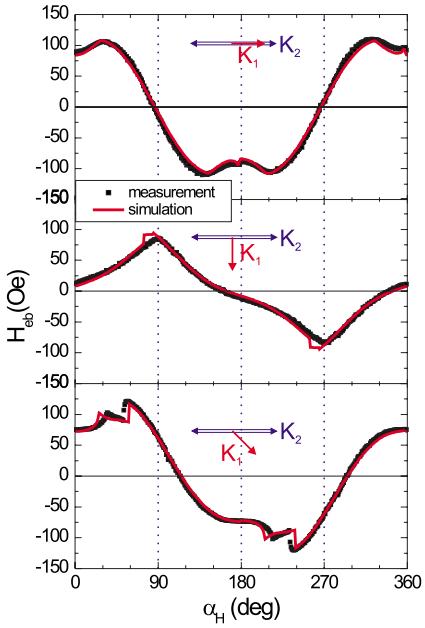

FIG. 3. (Color online) Angular dependence of H_{eb} (experiment: full symbols; simulation: line) for the same configurations as in Fig. 2 (top: $\alpha_{K_1}=1°$; middle: $\alpha_{K_1}=86°$; bottom: $\alpha_{K_1}=41°$).

obtained by means of longitudinal magneto-optic Kerr effect measurements.

The whole angular dependence of the magnetization reversal curves, measured and simulated, are shown in Fig. 2(a) for three different configurations of K_1 with respect to K_2, i.e., $\alpha_{K_1}=0°, 90°, 45°$. For all simulations the same anisotropy constants $K_1=7.9\times10^4$ erg/cm^3 and $K_2=2.8\times10^4$ erg/cm^3 are used. The only free parameter in the simulations is the mutual angle between both anisotropy contributions α_{K_1}, which has been set to 1° (left column), 86° (middle column), and 41° (right column), respectively. The small deviations in α_{K_1} from the nominal values are attributed to a misalignment during the field annealing procedure, which causes slight asymmetries in the angular dependence. With these values of anisotropy and α_{K_1} a perfect agreement between the experimental data and the numerical simulations is obtained simultaneously for all three configurations and also the experimental asymmetries are well reproduced. In addition, in Fig. 2(b) the measured and simulated magnetization reversal curves are shown for an in-plane angle of $\alpha_H=200°$ in a conventional way. Although both coercive fields are underestimated by the model in general, the exchange bias field, i.e., the loop shift, is reproduced perfectly. Its angular dependence, which has been extracted from the experimental and simulated magnetization reversal curves of Fig. 2, is shown in Fig. 3. Also this data representation demonstrates the perfect agreement between experimental data and the simulated angular dependence. The origin of minimal discrepancies are asymmetric deviations in coercivity. However, since no nucleation and domain-wall motion processes are considered in our model, the degree of congruence is still stunning.

The present results demonstrate that both anisotropy contributions are superimposed independently and that no interTABLE I. Unidirectional K_1 and uniaxial K_2 anisotropy contributions of exchange bias films deposited either on a flat or a rippled Si substrate. To further characterize the substrates the corresponding maximum step densities are given.

	Flat	Rippled
Step density (steps/nm)	$\leqslant 0.01$	≈ 0.7
Step distance (atomic units)	$\geqslant 500$	≈ 7
K_1 (erg/cm^3)	6.6×10^4	7.9×10^4
K_2 (erg/cm^3)	2.5×10^3	2.8×10^4

correlation between them is present. Furthermore, this also proves that dipolar effects arising from the film morphology exhibit only a negligible contribution to the unidirectional anisotropy and thus to the exchange bias effect. For a given interfacial roughness or step density the direction of the unidirectional anisotropy does not influence its magnitude. However, this finally leads to the question of whether the unidirectional anisotropy is influenced by the amount of interfacial roughness at all.

In order to address this issue, the same layer stack was deposited on a flat Si(001) substrate which has not been treated by ion erosion. After deposition both anisotropy constants have been determined using the same procedure as described above. In Table I the different anisotropy contributions are compared. The uniaxial anisotropy depends strongly on the step density and an increase by more than a factor of 10 is observed. In principle, this enhancement can have different microscopic origins: (i) dipolar effects due to the generation of stray fields,[21,22] or (ii) step-edge anisotropies due to reduced atomic coordination originating from spin-orbit coupling.[23,24] Based on Schlömann's theory[21] the dipolar contribution of one rough surface can be calculated by

$$K_2^{dip} = 2\pi M^2 \frac{\pi w^2}{\lambda D}$$

with w the rms roughness (0.74 nm), λ the periodicity (32 nm), and D the film thickness (9 nm). Using the experimental values we obtain $K_2^{dip}=2.8\times10^4$ erg/cm^3, exactly the value determined experimentally. However, since two interfaces are involved the calculated K_2^{dip} is even larger than K_2. In any case, it becomes immediately clear that the dipolar contribution governs the uniaxial anisotropy. In contrast to epitaxial systems,[16] the step-edge anisotropies are negligibly small. This can be understood considering the fact that the grains are oriented randomly in-plane and that consequently the step-edge orientation is random. The possible anisotropies arising from the step edges are thus canceled to a large extent.

In addition to the uniaxial anisotropy, also the unidirectional anisotropy is increased which can be attributed to an enhancement of uncompensated spins at the interface for a rippled interface with respect to a flat one. This is exactly what is expected[11] if a compensated antiferromagnet is considered. For uncompensated antiferromagnets a decrease in unidirectional anisotropy is predicted.[11] For the FeMn sys-

tem investigated here it is agreed that the magnetic ground state is the $3Q$ noncollinear magnetic structure, in which the magnetic moments align toward the center of the unit cell and thus create an ideally compensated antiferromagnetic material.[25,26] Consequently, the observed increase in unidirectional anisotropy is in full agreement with theoretical predictions.

In summary we have demonstrated that a ripple structure gives rise to an increase of both unidirectional and uniaxial anisotropy contributions in exchange bias systems in agreement with theoretical predictions. However, the origin of the increase is different for both cases; dipolar effects (uniaxial anisotropy) and uncompensated spins (unidirectional anisotropy). Since the direction of the unidirectional anisotropy can be set along any in-plane direction with its magnitude remaining unchanged intercorrelation effects between both anisotropies can be ruled out. The magnetization reversal behavior can be perfectly reproduced by an extended coherent rotation model for all different configurations simultaneously with one parameter set only.

The authors thank J. McCord for the critical reading of the manuscript. M.O.L. acknowledges the financial support from the European Communities Human Potential Program NEXBIAS under Contract No. HPRN-CT2002-00296.

*j.fassbender@fzd.de

[1] J. Nogues and I. K. Schuller, J. Magn. Magn. Mater. **192**, 203 (1999).
[2] R. L. Stamps, J. Phys. D **33**, R247 (2000).
[3] S. Riedling, M. Bauer, C. Mathieu, B. Hillebrands, R. Jungblut, J. Kohlhepp, and A. Reinders, J. Appl. Phys. **85**, 6648 (1999).
[4] T. Mewes, H. Nembach, M. Rickart, S. O. Demokritov, J. Fassbender, and B. Hillebrands, Phys. Rev. B **65**, 224423 (2002).
[5] H. Xi, T. F. Ambrose, T. J. Klemmer, R. van de Veerdonk, J. K. Howard, and R. M. White, Phys. Rev. B **72**, 024447 (2005).
[6] D. Y. Kim, C. G. Kim, C.-O. Kim, M. Shibata, M. Tsunoda, and M. Takahashi, IEEE Trans. Magn. **41**, 2712 (2005).
[7] S. Dubourg, J. F. Bobo, B. Warot, E. Snoeck, and J. C. Ousset, Phys. Rev. B **64**, 054416 (2001).
[8] J. Camarero, J. Sort, A. Hoffmann, J. M. Garcia-Martin, B. Dieny, R. Miranda, and J. Nogues, Phys. Rev. Lett. **95**, 057204 (2005).
[9] A. Hoffmann, M. Grimsditch, J. E. Pearson, J. Nogues, W. A. A. Macedo, and I. K. Schuller, Phys. Rev. B **67**, 220406(R) (2003).
[10] S. H. Chung, A. Hoffmann, and M. Grimsditch, Phys. Rev. B **71**, 214430 (2005).
[11] J.-V. Kim, R. L. Stamps, B. V. McGrath, and R. E. Camley, Phys. Rev. B **61**, 8888 (2000).
[12] C. Liu, C. Yu, H. Jiang, L. Shen, S. Alexander, and G. J. Mankey, J. Appl. Phys. **87**, 6644 (2000).
[13] K. Nakamura, A. J. Freeman, D.-S. Wang, L. Zhong, and J. Fernandez-de-Castro, Phys. Rev. B **65**, 012402 (2001).
[14] J. Erlebacher, M. J. Aziz, E. Chason, M. B. Sinclair, and J. A. Floro, Phys. Rev. Lett. **82**, 2330 (1999).
[15] B. Ziberi, F. Frost, Th. Höche, and B. Rauschenbach, Phys. Rev. B **72**, 235310 (2005).
[16] R. Moroni, D. Sekiba, F. Buatier de Mongeot, G. Gonella, C. Boragno, L. Mattera, and U. Valbusa, Phys. Rev. Lett. **91**, 167207 (2003).
[17] D. Sekiba, R. Moroni, G. Gonella, F. Buatier de Mongeot, C. Borgano, L. Mattera, and U. Valbusa, Appl. Phys. Lett. **84**, 762 (2004).
[18] F. Bisio, R. Moroni, F. Buatier de Mongeot, M. Canepa, and L. Mattera, Phys. Rev. Lett. **96**, 057204 (2006).
[19] A. L. Dantas, G. O. G. Reboucas, A. S. W. T. Silva, and A. S. Carrico, J. Appl. Phys. **97**, 10K105 (2005).
[20] E. C. Stoner and E. P. Wohlfarth, Philos. Trans. R. Soc. London, Ser. A **240**, 599 (1948).
[21] E. Schlömann, J. Appl. Phys. **41**, 1617 (1970).
[22] Y.-P. Zhao, G. Palasantzas, G.-C. Wang, and J. Th. M. De Hosson, Phys. Rev. B **60**, 1216 (1999).
[23] P. Gambardella, A. Dallmeyer, K. Maiti, M. C. Malagoli, W. Eberhardt, K. Kern, and C. Carbone, Nature (London) **416**, 301 (2002).
[24] S. Rusponi, T. Cren, N. Weiss, M. Epple, P. Buluschek, L. Claude, and H. Brune, Nat. Mater. **2**, 546 (2003).
[25] K. Nakamura, T. Ito, A. J. Freeman, L. Zhong, and J. Fernandez-de-Castro, Phys. Rev. B **67**, 014405 (2003).
[26] T. Mewes, B. Hillebrands, and R. L. Stamps, Phys. Rev. B **68**, 184418 (2003).